Geosci. Model Dev. Discuss., 5, 149–188, 2012
www.geosci-model-dev-discuss.net/5/149/2012/
doi:10.5194/gmdd-5-149-2012

Geoscientific Model Development Discussions

Implementation and evaluation of online gas-phase chemistry within a regional climate model (RegCM-CHEM4)

A. K. Shalaby[1,2], A. S. Zakey[1,2,3], A. B. Tawfik[4], F. Solmon[1], F. Giorgi[1], F. Stordal[5], S. Sillman[4], R. A. Zaveri[6], and A. L. Steiner[4]

[1]Earth System Physics Group, International Centre for Theoretical Physics, Trieste, Italy
[2]Egyptian Meteorological Authority (EMA), Cairo, Egypt
[3]Danish Meteorological Institute (DMI), Copenhagen, Denmark
[4]Department of Atmospheric, Oceanic and Space Sciences, University of Michigan, Ann Arbor, Michigan, USA
[5]Department of Geosciences, University of Oslo, Norway
[6]Atmospheric Sciences and Global Change Division, Pacific Northwest National Laboratory, Richland, Washington, USA

Received: 1 January 2012 – Accepted: 5 January 2012 – Published: 17 January 2012

Correspondence to: A. L. Steiner (alsteiner@umich.edu)

Published by Copernicus Publications on behalf of the European Geosciences Union.

Abstract

The RegCM-CHEM4 is a new online climate-chemistry model based on the International Centre for Theoretical Physics (ICTP) regional climate model (RegCM4). Tropospheric gas-phase chemistry is integrated into the climate model using the condensed version of the Carbon Bond Mechanism (CBM-Z; Zaveri and Peters, 1999) with a fast solver based on radical balances. We evaluate the model over Continental Europe for two different time scales: (1) an event-based analysis of the ozone episode associated with the heat wave of August 2003 and (2) a climatological analysis of a six-year simulation (2000–2005). For the episode analysis, model simulations show good agreement with European Monitoring and Evaluation Program (EMEP) observations of hourly ozone over different regions in Europe and capture ozone concentrations during and after the August 2003 heat wave event. For long-term climate simulations, the model captures the seasonal cycle of ozone concentrations with some over prediction of ozone concentrations in non-heat wave summers. Overall, the ozone and ozone precursor evaluation shows the feasibility of using RegCM-CHEM4 for decadal-length simulations of chemistry-climate interactions.

1 Introduction

The role of atmospheric chemistry in the climate system is now recognized as being of central importance (IPCC, 2007). Climate-chemistry interactions and the evolution of air quality over the coming decades depend on many factors, such as the growth of pollutant emissions due to worldwide economic development, localized emissions in high activity areas such as megacities, and changes in climatic factors such as temperature and precipitation. Many recent studies have focused on the impact of increased greenhouse gas concentrations on air quality and have generally found an increase in tropospheric ozone as temperatures and greenhouse gas concentrations increase (e.g., Weaver et al., 2009; Zhang et al., 2009; Leibenspeger et al., 2008;

GMDD
5, 149–188, 2012

Hedegaard et al., 2008; Solberg et al., 2008; Struzewska and Kaminski, 2008; Meleux et al., 2007; Giorgi and Meleux, 2007; Forkel and Knoche, 2006; Hodzic et al., 2006; Stevenson et al., 2005; Langner et al., 2005; Meehl and Tebaldi, 2004; Vautard et al., 2005; Ordonez et al., 2005). Specifically, ozone is an important component in the troposphere because (1) it is a leading indicator of poor air quality that adversely affects human health and natural ecosystems (e.g. WHO, 2003) and (2) has the ability to act as a greenhouse gas. However, simulations of tropospheric ozone can be complex because it is a relatively short-lived species with a lifetime of approximately several days to weeks and exhibits a broad spatial heterogeneity (Jacob and Winner, 2009).

A number of chemistry-climate models with various levels of offline and online coupling between the chemistry and atmospheric dynamics have been developed to investigate the interactions between climate and air quality (reviewed in Zhang, 2008). "Offline" coupling uses the meteorological output from weather or climate models to drive chemistry transport models, requiring two separate model simulations to study the effects of climate on air quality. Offline regional coupling has been more widely used and many studies have addressed the issue of the effects of climate change on regional ozone concentrations using the offline method (e.g., Langner et al., 2005; Szopa et al., 2006; Steiner et al., 2006; Meleux et al., 2007; Krüger et al., 2008; Liao et al., 2009; Chen et al., 2009). However, a preferred method to address issues of chemistry-climate interactions is to use fully coupled or "online" chemistry-climate models. Online methods directly transmit meteorological fields produced by the climate model to a chemistry module and calculate the concentration of climate-relevant tracers. The radiative forcing of these tracers then feeds back into the climate model to affect temperatures and regional circulation. This technique is optimal yet computationally demanding, because ozone formation chemistry is complex and requires a large number of species to be tracked in a three-dimensional framework. Most online coupled chemistry-climate models are global scale with coarse spatial resolutions (e.g., Emmons et al., 2010). Computational and physicochemical complexity has thus prevented the widespread implementation of high-resolution, coupled chemistry-climate

GMDD
5, 149–188, 2012

models for long-term climate integrations. To date, only a few regional climate models (RCMs) include online coupling with a range of chemical complexity (e.g., Jacobson et al., 1996, 1997a, b; Qian and Giorgi, 1999; Grell et al., 2005; Forkel and Knoche, 2006; Solmon et al., 2006; Zhang et al., 2010).

The intent of RegCM-CHEM4 model development presented here is to accurately simulate ozone while allowing for decadal-scale climate simulations. Here we discuss the gas-phase chemistry development and provide a first assessment of the coupled model performance over a European regional domain. We assess the ability of the RegCM-CHEM4 to simulate ground-based ozone and its precursors for (1) a short-term model evaluation for the heat wave of August 2003 and (2) an analysis of a six-year simulation to assess the suitability for long-term climate simulations. For the one month case study, we select the summer of 2003 because it was one of the hottest on record in Europe (Schär et al., 2004). June-July-August (JJA) average temperatures were more than 5 K warmer than the 1961–1990 average (Fink et al., 2004) and exceeded the next highest anomaly by a factor of two in some locations (Schär et al., 2004). During this time period, ozone concentrations were extremely high due to the anomalous weather patterns (e.g., Vautard et al., 2005; Struzewska et al., 2008; Solberg et al., 2008), contributing to health crises in several countries and triggering drought and a crop shortfall in Southern Europe. These temperature and ozone maxima make it an optimal test case to evaluate the simulations of climate-chemistry interactions. Section 2 provides a basic description of the relevant climate and chemistry components of RegCM-CHEM4. Section 3 describes the model simulation of the ozone episode associated with the 2003 heat wave over Europe and Sect. 4 includes an analysis of six-year simulations over the same domain to illustrate that the model is suitable for long-term simulations. We conclude in Sect. 5 by addressing the uncertainties in the coupled model, plans for future work, and a guideline for use in future studies.

GMDD
5, 149–188, 2012

2 Model description

2.1 Regional climate model version 4 (RegCM4)

The climate component of the coupled model is the RegCM4, a model developed and maintained at the Abdus Salam International Centre for Theoretical Physics (ICTP) for over a decade (Pal et al., 2007; Giorgi et al., 2012). RegCM4 is a hydrostatic, sigma coordinate model described in Giorgi et al. (2012), which has been used for a wide range of applications across the globe (Giorgi and Mearns, 1999; Giorgi et al., 2006). There are several options for the parameterization of model physics and in the simulations presented here, we employ the mass-flux cumulus scheme of Grell (1993), the resolvable precipitation scheme of Pal et al. (2000), the non-local planetary boundary layer parameterization of Holtslag and Bouville (1993), and the radiation scheme of the CCM3 (Kiehl et al., 1996, in the implementation of Giorgi and Shields, 1999). Surface processes are treated using the Community Land Model version 3.5 (Oleson et al., 2008; Tawfik and Steiner, 2011). The reader is referred to Giorgi and Mearns (1999b), Pal et al. (2007) and Giorgi et al. (2012) and references therein for a more detailed description of RegCM4. The simulations presented here use a dynamical model time step of 200s with the land model called every 600 s.

2.2 Trace gas continuity equation

Prior RegCM versions have implemented a chemical transport scheme to study the transport, fate and radiative impact of atmospheric aerosols (e.g., Qian and Giorgi, 1999; Solmon et al., 2006). In this study, we modify the RegCM4 chemical transport module to include gas-phase species using a mass continuity equation for each tracer (i) mixing ratio χ (Solmon et al., 2006):

$$\frac{\partial \chi^i}{\partial t} = -V \cdot \nabla \chi^i + F^i_{\mathrm{H}} + F^i_{\mathrm{V}} + T^i_{\mathrm{cum}} + S^i_{\mathrm{r}} - R^i_{\mathrm{w,ls}} - R^i_{\mathrm{w,cum}} - D^i_{\mathrm{dep}} + R^i_{\mathrm{net}} \quad (1)$$

GMDD
5, 149–188, 2012

The first term in the right hand side of Eq. (1) is the horizontal and vertical advection of χ, F_H and F_V are horizontal and vertical turbulent diffusion, respectively; T_{cum} is the vertical transport by cumulus clouds, S_r is the emission term, $R_{w,ls}$ and $R_{w,cum}$ are the wet removal terms by resolvable scale and cumulus precipitation, respectively, D_{dep} is the dry deposition, and R_{net} is the net production by gas-phase reactions. Advection, diffusion, and cumulus transport are parameterized as in Solmon et al. (2006). Dry and wet deposition parameterizations are discussed in Sect. 2.5. By solving this equation within the RegCM dynamical core, we can account for the online, coupled simulation of atmospheric chemistry and climate.

We solve the tendency equation (Eq. 1) sequentially in two steps. In the first step, all processes except R_{net} are solved using the leapfrog scheme, while in the second step we solve the R_{net} term. This method provides the ability to run the chemistry with a longer time step than that of the other processes. The chemistry mechanism is called every 1000 s or fifth model time step and calculates the chemistry tendency for each tracer species. This chemistry tendency is then applied to every time step when the chemistry module is not called to produce a smooth chemical tracer time evolution. In the simulations presented here, aerosol transport is not included though has been tested and integrated with the gas-phase chemistry in other simulations.

2.3 Gas phase mechanism and solver

Prior work tested several atmospheric chemistry mechanisms in the model (results not shown) and in this study, we select the photochemical mechanism CBM-Z (Carbon Bond Mechanism; Zaveri and Peters, 1999) because it affords a reasonable trade-off between accuracy and computational efficiency. CBM-Z is based on the widely used CBM-IV scheme (Gery et al., 1989) developed for use in urban air-shed models for air quality applications. While both CBM-IV and CBM-Z use lumped species that represent broad categories of volatile organic compounds (VOC) based on carbon bond structure, CBM-Z also includes species and reactions that are important at regional to global scales and longer time periods than the typical urban airshed simulations.

GMDD
5, 149–188, 2012

CBM-Z has been extensively used in atmospheric chemistry simulations and interpretation of field measurements collected over urban (Zaveri et al., 2003; Jiang and Fast, 2004; Fast et al., 2006; Zaveri et al., 2010a,b) and regional (Fast et al., 2002; Fast and Heilman, 2005) areas.

Calculating the time evolution of gas-phase chemistry requires numerically integrating a set of stiff ordinary differential equations and is among the most computationally expensive operations performed in a photochemical grid model. A suite of numerical procedures with efficient solutions has been developed (e.g., Jacobson, 1996), and here we apply the computationally rapid radical balance method (RBM) of Sillman et al. (1991) and Barth et al. (2002) to solve the tendency equation for photochemical production and loss. RBM utilizes the fact that much of the complexity of tropospheric chemistry stems from the OH radical and the HO_x radical family (OH, HO_2 and RO_2) having a limited set of sources and sinks. The method solves reverse-Euler equations for OH and HO_2 based on the balance between sources, sinks and (if applicable) prior concentrations at the start of the time step. Reverse Euler equations for other species are solved in a reactant-to-product order, in some cases involving pairs of rapidly interacting species, and with some modifications to increase accuracy in exponential decay situations. The procedure is equivalent to a reverse Euler solution using sparse-matrix techniques, but with the matrix inversion linked specifically to the behaviour of OH and other species in the troposphere.

2.4 Photolysis rates

Photolysis rates are determined as a function of several meteorological and chemical inputs including altitude, solar zenith angle, overhead column densities for O_3, SO_2 and NO_2, surface albedo, aerosol optical depth, aerosol single scattering albedo, cloud optical depth and cloud altitude. Rates for specific conditions are interpolated from an array of pre-determined values based on the Tropospheric Ultraviolet-Visible Model (TUV) developed by Madronich and Flocke (1999) and based on a pseudo-spherical discrete ordinates method (Stamnes et al., 1988) with 8 streams. The 8-stream TUV is

GMDD
5, 149–188, 2012

an accurate method for determining photolysis rates but is computationally too expensive for online application in 3-D models; therefore, we use tabulated and interpolated values in our simulations.

Photolysis rates can be significantly affected by the presence of clouds. The method used to correct for cloud cover is based on Chang et al. (1987), which requires information on cloud optical depth for each model grid cell. Optical depth is used to reduce photolysis rates for layers within or below clouds to account for UV attenuation or to increase photolysis rates due to above-cloud scattering. The correction of clear-sky values depends on whether the location is below, above, or within the cloud. Cloud optical depths and cloud altitudes from RegCM-CHEM4 are used in the photolysis calculations, thereby directly coupling the photolysis rates and chemical reactions to meteorological conditions at each model time step. The adjustment to clear sky photolysis rate for below and within the cloud layer is:

$$J_{\text{cloud}} = J_{\text{clear}}\left[1 + F_{\text{c}}(1.6\tau_{\text{r}}\cos\theta - 1)\right] \quad (2)$$

where F_{c} is cloud cover fraction, θ is the zenith angle, and τ_{r} is the cloud transmissivity (calculated as a function of the cloud optical depth). In general, below cloud photolysis rates will be lower than the clear sky value due to the reduced transmission of radiation through the cloud. Similarly, photolysis rates are enhanced above the cloud due to the reflected radiation from the cloud as follows:

$$J_{\text{above}} = J_{\text{clear}}\left[1 + F_{\text{c}}((1 - \tau_{\text{r}})\cos\theta)\right] \quad (3)$$

2.5 Deposition

Dry deposition is the primary removal process for trace gas species in the model, and is parameterized as three resistances in series: (1) aerodynamic resistance, (2) quasi-laminar sub-layer resistance and (3) bulk surface resistance that accounts for stomatal and non-stomatal uptake in plants and soil. Dry deposition is modelled for 29 gas phase species following the CLM4 dry deposition model (based on the Wesley (1989) dry

GMDD
5, 149–188, 2012

deposition scheme), where the CLM land cover types are converted into the 11 Wesley land cover types. In the dry deposition scheme we consider both stomatal and non-stomatal resistances, which is necessary as the stomatal uptake occurs only during the daytime for most chemical species. This leads to a more accurate representation of diurnal variations of dry deposition, a process crucial for climate-chemistry interactions. All resistances are calculated in the CLM land surface model, resulting in consistent modelled values with the simulated land-atmosphere meteorology.

Wet deposition is parameterized as in the MOZART global model (Horowitz et al., 2003; Emmons et al., 2010). In our simulations, we include the removal of for 26 CBM-Z gas phase species based on the amount of large-scale precipitation as generated by the RegCM precipitation parameterization. Current simulations do not include wet removal by cumulus precipitation but this inclusion is planned for future model versions. Because the August 2003 event was exceptionally dry, we do not expect that this will significantly impact our wet removal rates during the event analysis.

2.6 Emissions inventories

Emissions inventories implemented in RegCM-CHEM4 include anthropogenic emissions, emissions from biomass burning and natural emissions from the biosphere (or biogenic emissions) (Fig. 1). These inventories vary greatly in terms of spatial (typically $1^{\circ} \times 1^{\circ}$ or $0.5^{\circ} \times 0.5^{\circ}$ in the horizontal) and temporal resolution (annually and monthly). The RegCM framework is designed for implementation over any regional-scale domain in the world, therefore we develop an emissions pre-processor dataset that optimizes the spatial and temporal scales of the available coarse inventories and are be adaptable to any location. We note that the use of these inventories results in relatively coarser grids than used in many regional air quality models, which are often developed for specific source regions by local, state and federal agencies. The pre-processor code re-grids and interpolates the emissions data to the same model projection and resolution as needed by RegCM-CHEM4 and unifies the emission units for different inventories. The simulations presented in this manuscript include the MACCity emissions, which

GMDD
5, 149–188, 2012

is an extension of the ACCMIP emissions dataset for 1990–2010 (Lamarque et al., 2010). This $0.5^{\circ} \times 0.5^{\circ}$ inventory represents annual changes in anthropogenic emissions and monthly inventories for biomass burning over the simulation years (2000–2005). Biogenic emissions are calculated in an online biogenic VOC model (the Model of Emissions of Aerosols and Gases from Nature (MEGAN); Guenther et al., 2006) implemented online in RegCM with CLM (Tawfik et al., 2012). The online biogenic emissions use modelled temperature, radiation and soil moisture allowing for a consistent inventory based on modelled meteorology and climatology.

Monthly emissions inventories are employed in the model and we note that daily and diurnal variations are not prescribed in the anthropogenic emissions inventories, which may impact the daily minima and maxima ozone concentrations. Centres of high anthropogenic industrial emissions (indicated with NO_x and alkane emissions) are concentrated near urban areas in Germany, France and the UK (Fig. 1a,b). Biomass burning emissions are most pronounced in Portugal, Northern Poland and in many of the Italian and Greek Mediterranean areas during August 2003 (Fig. 1c). August biogenic emissions are localized near forested areas, with the largest emissions in Central Europe in France, Germany and Northern Spain (Fig. 1d). For the climatological simulations, the biomass burning emissions and biogenic VOC emissions exhibit a strong seasonal cycle and are close to zero during the winter months.

2.7 Simulation design

To test the ability of the coupled RegCM-CHEM4 to simulate ozone, we conduct one simulation for 6.5 yr from 1 June 1999–31 December 2005. The first six months of the simulation is for climate model spin up and is not included in the analysis time period of 2000–2005. The heat wave event analysis evaluates hourly output from the month of August 2003 (Sect. 3) and the climatological ozone analysis evaluates the simulation of ozone for the full six-year time period (1 January 2000–31 December 2005; Sect. 4). The model domain (Fig. 1) has a horizontal resolution of 60 km × 60 km and 18 vertical levels. Because RegCM4 is a limited-area model, meteorological lateral

GMDD
5, 149–188, 2012

boundary forcings are required. For present-day simulations such as the one here, initial and lateral boundary conditions for the meteorological fields are provided by ERA-Interim analysis every six hours with weekly ERA sea surface temperatures (Dee et al., 2011). Climatological chemical boundary conditions are provided by the global, three-dimensional MOZART chemical transport model by using a monthly average of years 2000–2007 (Horowitz et al., 2003; Emmons et al., 2010). This model setup allows the evaluation of modelled versus measured ozone concentrations on a realistic basis for short-term event simulations in a regional weather-air quality framework (Sect. 3) and also for longer integrations as a regional climate-air quality model (Sect. 4). To provide computational context, the 6.5-yr simulation for this domain using 45 processors required 47 h and 20 min of computation time.

3 2003 European ozone event

3.1 Meteorological conditions

Maximum temperatures of 308–313 K were repeatedly recorded in July and the first half of August across Europe in 2003. As noted in several other studies (e.g., Beniston et al., 2004; Black et al., 2004), these extreme weather conditions were caused by an anti-cyclone positioned over Western Europe, blocking the rain-bearing depressions originating over the Atlantic Ocean from reaching the continent. This exceptional length of these stagnant conditions (over 20 days) increased the flow of very hot, dry air from sub tropical regions to Europe. The extreme event and the anomalously warm and dry conditions increased ozone concentrations over Europe to unusually high values (Vautard et al., 2005; Meleux et al., 2007; Solberg et al., 2008).

The ERA-Interim reanalysis data (interpolated to model grid; Fig. 2a) displays this pattern and the RegCM-CHEM4 accurately simulates this high pressure and anti-cyclonic circulation over Europe (Fig. 2b). RegCM-CHEM4 places the center of the anti-cyclonic feature in approximately the same location as the driving reanalysis, yet

GMDD
5, 149–188, 2012

simulates slightly stronger winds over Central and Northern Europe. Outflow from Central Europe to the Mediterranean is slightly stronger in the RegCM than the reanalysis. Because the RegCM-CHEM4 is driven by ERA-Interim boundary conditions (updated every six hours), this agreement is not surprising but we note this pattern to show that the interior model domain replicates the main meteorological features leading to the high ozone event. This circulation pattern is also conducive to subsidence conditions that favour ozone accumulation over the continent (Vautard et al., 2005).

During August 2003, RegCM-CHEM4 simulates surface air temperatures of 290–296 K over Continental Europe, with temperatures increasing up to 303 K in the Iberian Peninsula and Italy (Fig. 3a). Comparisons with gridded observational data (Mitchell and Jones, 2005) show that RegCM-CHEM4 reproduces the main temperature patterns relative to CRU observational data for August 2003 (Fig. 3b) with a warm bias in the western portion of France, the Alps and Central Italy of up to 4 K. Throughout the rest of the model domain, the bias is within 1–2 K. Overall, Figs. 2 and 3 demonstrate the ability of the RegCM to simulate the main meteorological features that led to the high ozone episode over Europe in early August 2003.

3.2 Ozone episode development

Corresponding to surface ozone measurements, first layer (approximately 50–100 m height) simulated ozone concentrations at 14 UTC for selected days (1, 4, 8, 10, 12, 16 August) are compared to ozone surface observations from the European Monitoring and Evaluation Programme (EMEP) station network (http://www.emep.int; Fig. 4). The production of ozone is affected by meteorology as described in Sect. 3.1, yet is very sensitive to the location and magnitude of emissions and the resulting VOC/NO_x ratio. In the first two days of August, maritime westerly flow over Western Europe leads to low to moderate ozone concentrations (40–60 ppb) in Northern and Central Europe, with slightly higher concentrations in Eastern France and Germany. Observations in Germany show elevated concentrations of 100–130 ppb (Fig. 4a). The model simulates this increase in the region, although with slightly lower concentrations (85–95 ppb) and

GMDD
5, 149–188, 2012

a location displaced slightly to the west. Additionally, the model overestimates ozone over the UK with simulated values of 85–95 ppb as compared to observed values of 40–60 ppb, particularly in the northern portion of the island in the first several days of the simulation.

During 3 and 4 August, ozone builds up in the boundary layer with concentrations exceeding the European standards (90 ppb) south and southwest of the Ruhr region and over Central France (Fig. 4b). The anticyclonic circulation causes the high ozone region to shift clockwise from Southern Germany on 4 August to Central France on 6–7 August, and then to Western France on 8–10 August (Fig. 4c and 4d). On 11–12 August, very high ozone levels occur over most of France and Western Europe (Fig. 4e) while after 15 August, the polluted air mass is pushed eastward by a front coming from the Atlantic (Fig. 4f). The model captures the movement of this feature with measured and modelled concentrations matching fairly well on 8 August (Fig. 4c). On 12 August (Fig. 4e), the model produces high concentrations in Central Germany, though measurements at this hotspot are lacking and surrounding observations are greater than modelled concentrations by about 20 ppb. These elevated concentrations begin to dissipate on 15 August towards Eastern Europe (Fig. 4f), whereas the limited observations suggest that concentrations shift slightly back to the east over Switzerland. Despite these small differences in concentrations, the model reproduces the circulation of ozone fairly well. Similar ozone concentration magnitudes and positioning were noted by Vautard et al. (2005).

3.3 Ozone time series analysis

To further examine the simulation of the 2003 August event ozone, we compare hourly observed surface ozone concentrations from EMEP stations with modelled ozone concentrations (Fig. 5) for four regions: (1) a selection of eight representative European stations noted by Solberg et al. (2008) including: Donon (FR08), Revin (FR09), Morvan (FR10), Peyrusse-Vieille (FR13), Campisabalos (ES09), Kosetice (ZC03), Waldhof (DE02), and Ueckermünde (DE26; this station replaces the Zingst site due to lack of

GMDD
5, 149–188, 2012

data availability), (2) stations located in Northern Europe (defined as all EMEP sites north of 50° N), (3) stations in Central Europe (EMEP sites within the latitude range of 47–50° N), and (4) stations in Southern Europe (EMEP stations south of 47° N).

When averaged over the eight representative stations, the model captures the observed diurnal evolution of the ozone episode (Fig. 5a). Daily minima and maxima are well reproduced by the model with biases less than 5 ppb. Most notably, RegCM-CHEM captures the sharp decrease in daily ozone maxima from 70–80 ppb during the early August event to 50–60 ppb at the end of the event on 14 August. After this date, modelled concentrations are greater than observed with a daily maximum bias of 5–10 ppb. In the Northern Europe region (sites north of 50° N), measured-modelled agreement is also strong with daily maxima typically within 5 ppb of observed concentrations. During the ozone event in the northern region, the model predicts ozone minima up to 12 ppb greater than observed, however this bias is reduced after the passage of the frontal system on 15 August. In the Central European region (47–50° N), the model captures the diurnal variations over the month of August yet frequently underestimates the ozone maxima during the main part of the event (Fig. 4c). After the heat wave breaks on 14 August, ozone concentrations are sometimes greater than observed and sometimes less; no clear bias is evident. In the southern region, the model underestimates the ozone maxima in the latter half of the heat wave event (6–12 August), yet overestimates the maxima in the second half of the month. After the heat wave, modelled ozone minima are also higher than observed, showing a shifted diurnal cycle in the model to higher concentrations.

To evaluate potential sources of O_3 model bias, we examine the diurnal cycles of modelled rates of net chemical production (ozone production – loss; ppb h^{-1}) for each region during and after the ozone event (Fig. 6). During the event (1–14 August 2003), chemical production is highest (up to 5 ppb h^{-1}) in the central region and over the 8-station average. Comparatively, net production rates during the daytime are smaller for the northern and southern regions (~ 3 ppb h^{-1}), yet night time loss rates are much higher in the northern region likely due to the titration of O_3 by high NO_x emissions

GMDD
5, 149–188, 2012

in this region. This increase in night time chemical loss may be biased by the lack of diurnal cycle in NO_x emissions; however we note that we still observe an overestimation of the night time minima in the northern region suggesting that it is not causing large problems in our model bias. Dry deposition rates for O_3 are greater in the central region and the 8-station average and are driven by high atmospheric concentrations in these regions, with deposition decreasing in the northern and southern region where ozone surface concentrations are lower. After the event (16–31 August), daytime chemical production rates drop by about 40–60 % in the central and 8-station regions and are halved in the northern region, with little change in night time net chemical loss of O_3. This explains the event-based changes in Fig. 5, with higher ozone concentrations during the event and decreasing after the event. The southern region does not show as strong a shift in O_3 concentrations after the event as other regions (Fig. 5), reflected in small changes in the net production rate during and post-event ($\sim$ 10%) and could be attributed to the increased role of biogenic VOC in this region. Dry deposition rates decrease by about 25–40 % after the event in the central and 8-station region, with greater decreases in the north (60 %) and smaller reductions in the South (30 %). Overall, both changes in chemistry and deposition contribute to the decrease in ozone concentrations after the event.

We note that there are several physical and emissions processes that could be contributing to these modelled-observed discrepancies. First, as noted in Sect. 3.1 and Fig. 3, there is a slight warm bias in RegCM-CHEM4 particularly in the Southern Mediterranean, which could amplify the online isoprene emissions and ozone formation and lead to higher modeled concentrations than observed. For example in the central and southern regions, the model tends to simulate more ozone than observed in the second half of August 2003. Other studies have noted the role of drought stress during this time period, where the heat and drought stress over Europe have been postulated to increase stomatal closure, reduce dry deposition and increase ambient ozone concentrations (Solberg et al., 2008). Our simulations are slightly warmer than observed and because of the coupled land-atmosphere nature of the RegCM model,

GMDD
5, 149–188, 2012

they likely capture this drought-deposition feedback and are not likely the cause of our ozone biases.

3.4 Ozone precursors

An evaluation of ozone precursors including NO_2 concentrations and two select VOC species can provide further insight into model behaviour, although we note the reduced sampling frequency in both space and time for VOC from the EMEP network. Most VOCs are only measured twice per week and there is lack of data from multiple stations during August 2003. Furthermore, it is difficult to make direct comparisons of the lumped VOC species in CBM-Z with measured VOC. Therefore, we compare two VOC species important for our analysis: (a) isoprene, a primary biogenic emission and (b) formaldehyde (HCHO), an oxygenated VOC that can result from primary anthropogenic emissions but its dominant source in the atmosphere is via the oxidation of anthropogenic and biogenic VOC.

Figure 7 shows a time series of August 2003 NO_2 observations versus observations, spatially grouped in the same manner as the ozone evaluation (Fig. 5). This includes the "eight representative stations", where only one of these eight stations measures NO_2 (ES09), Northern Europe (10 stations), Central Europe (1 station), and Southern Europe (11 stations). In general, the model predicts a regular diurnal cycle with higher concentrations than observed. Additionally, the model frequently misses high-concentration events present in the observations. This is not surprising because the model's daily variability is driven by meteorology as emissions only vary on the monthly time scale. Observed values range from 4–12 ppb in Northern Europe, 4–20 ppb in Central Europe, and 1–7 ppb in Southern Europe. At the ES09 station, the model over predicts NO_2 concentrations by several ppb over most of the month and also slightly underestimates night time NO_2 by 0.5–2 ppb. At the Northern European stations, the model overestimates daily maxima by 10–20 ppb, with reduced biases at the Central and Southern Europe stations. The single Central Europe site has the greatest NO_2 concentrations (ranging up to 20 ppb) with decreasing values in Southern Europe, and

GMDD
5, 149–188, 2012

the model reproduces these broader spatial patterns. As noted above, the model is designed for climatological simulations and uses monthly emissions, therefore we would not expect to reproduce these daily events with any fidelity. Figure 7 does indicate, however, that the model generally represents the proper spatial range of NO_2 concentrations and this likely leads to the good measured-modelled agreement of ozone concentrations as discussed in Sect. 3.3.

VOC measurements at the EMEP stations are more limited than NO_2, with a total of 11 stations reporting VOC data and 8 stations reporting carbonyl data in our model domain. Because of these limits in space and time, scatter plots compare observed isoprene concentrations versus modelled concentrations at twelve stations in August 2003 (Fig. 8a–c) and observed HCHO concentrations versus modelled HCHO (Fig. 8d–f). Isoprene is a predominantly biogenically emitted species with online model emissions, meaning that RegCM temperature, radiation, and soil moisture data are used to drive hourly emission calculations. Observed isoprene concentrations range from 0–1.2 ppb in Northern Europe, 0–0.5 ppb in Central Europe, and up to 4.5 ppb in Southern Europe. The model captures these general regional trends, although the scatter is high and R^2 values are extremely low. In Southern Europe, modelled concentrations are about a factor of two higher than observed. We attribute this model overestimate to the warm temperature bias present in RegCM-CHEM4, which can increase the amount of biogenic isoprene emitted due to the online emissions scheme.

Measured HCHO values range up to 6–8 ppb in Northern and Central Europe, with slightly lower values in the Southern Europe (up to 4 ppb) (Fig. 8d–f). Higher values in Northern and Central Europe suggest an anthropogenic oxidation component to observed concentrations, as these are collocated with many of the primary anthropogenic VOC emissions. In all regions, the model underestimates observed concentrations by a factor of 2–4. With only few ground-level observations to evaluate, it is difficult to pinpoint the cause of these discrepancies, but they suggest that oxidation in the model may be too slow particularly in the more urbanized regions of Northern and Central Europe.

GMDD
5, 149–188, 2012

3.5 VOC and NO_x sensitivity

Past studies have evaluated the sensitivity of ozone formation in Europe to the two main ozone precursors and have noted that Northwestern Europe is typically VOC-sensitive transitioning to NO_x-sensitive to the south (Beekman and Vautard, 2010). To evaluate the model response to the ozone precursors and determine if we can replicate these regional sensitivities, we evaluate simulated NO_y concentrations as a proxy for ozone sensitivity as it correlates well with other detailed sensitivity studies in Europe (Beekman and Vautard, 2010). Here we define NO_y as the sum of NO_2+NO+HNO_3+PAN, where relatively high concentrations can provide an indicator of VOC-sensitive regions. Additional reactive nitrogen species (e.g., alkyl nitrates, isoprene nitrates, and higher order PAN analogues) would increase NO_y by approximately 25% if included.

Previous studies have shown that NO_x-sensitive conditions are generally associated with low values of NO_y during the afternoon (concurrent with the time of elevated O_3) and that VOC-sensitive conditions are associated with higher NO_y (Milford et al., 1994; Sillman and He, 2002; Beekman and Vautard, 2010). The NO_y threshold for VOC- versus NO_x-sensitivity can vary depending on location, with inter-regional differences caused by the overall VOC/NO_x ratio, meteorological conditions, and the influence of ozone advection. In the United States, VOC-sensitive conditions have been defined as NO_y=11–50 ppb and NO_x-sensitive locations displaying NO_y=3–12 ppb (Milford et al., 1994). In Europe, these values have been determined to be slightly lower than the United States and VOC-sensitive regimes have been noted as 6–13 ppb in Southwestern Germany (Vogel et al., 1999) and ranging from 6–9 ppb depending on location in Continental Europe (Beekman and Vautard, 2010).

Figure 9 shows the distribution of NO_y at the peak of the ozone episode (average 14:00 UTC concentration in August 2003). High NO_y concentrations are generally located near the main NO_x sources in the model, including Southern British Isles, the Benelux states and Western Germany as well as few locations in Northern Italy and the south of France. This suggests that the model is VOC-sensitive in the southern

GMDD
5, 149–188, 2012

portion of the British Isles and across some of Northern Europe, as noted in other studies (Beekmann and Vautard, 2010). NO_y concentrations in Spain and the southern portion of Italy are lower (typically less than 6 ppb) suggesting NO_x-sensitivity in this region. The apparent plume of high NO_y extending south into the Mediterranean from the coast of France is noteworthy. This plume corresponds to reduced O_3 relative to the surrounding region and most likely represents slower formation of O_3 in a high NO_x plume. Elevated NO_x in urban plumes transported over water have been attributed to the combination of high NO_x emission near the shoreline and suppressed vertical mixing over water (Sillman et al., 1993; Neuman et al., 2006). In general, the distribution of NO_y concentrations look similar to other regional chemistry models (e.g., Beekman and Vautard, 2010), with the exception of emissions along the southern coast of France extending out over the Mediterranean. This area has the highest NO_y concentrations in the model domain and is likely due to the relatively high NO_x source in the region from our selected inventory. Overall, these results suggest that the model is simulating the proper photochemical regimes necessary to capture ozone formation.

4 Climatological ozone simulation

The 2003 European ozone event analysis presented in Sect. 3 indicates that the model simulates ozone well compared to observations for short-term (e.g., event-based) analysis. Here we evaluate results from a continuous six-year integration over the same domain to provide evidence of the RegCM-CHEM4's ability to perform long-term simulations of ozone. Modelled seasonal average surface air temperatures for winter (DJF) and summer (JJA) show the seasonal cycle of temperature (Fig. 10a and b), with modelled biases as comparisons to CRU gridded temperatures (Fig. 10c and d). Winter biases in Continental Europe typically are less than 2 K, with a warm bias in Northern Scandinavia and Eastern Europe of 3–5 K and a slight cool bias over Northern Africa of 3–4 K. In summer (Fig. 10d), a slight warm bias (less than 2 K) exists throughout Continental Europe, with a stronger warm bias over the Alps and Central Italy (3–6 K).

GMDD
5, 149–188, 2012

Overall, however, the temperature biases in RegCM remain small over much of the ozone evaluation region with the exception of the high-altitude areas in the Alps.

To evaluate the modelled ozone concentrations from the long-term climate simulations, we implement the ground-based EMEP ozone measurements as described in Sect. 3 for the August 2003 analysis, including the eight representative stations, Northern Europe (30 stations), Central Europe (28 stations), and Southern Europe (25 stations). We compare modelled monthly average daily maxima with ground-based EMEP observations over the six years of analysis (2000–2005) for each of the regions (Fig. 11). For the eight representative stations, the model over predicts ozone concentrations in most of the summers except for the 2003 heat wave event, where measured and modelled concentrations have similar average monthly summertime maxima (70 ppb). Modelled wintertime concentrations are within 5 ppb of observed values ($\sim$ 30 ppb). In the Northern Europe region, the measurements show a bi-modal peak in the ozone maxima, with the highest concentrations in the early summer (up to 50 ppb), then decreasing in the midsummer to about 45 ppb, then increasing again slightly in late summer. The model does not reproduce this bi-modal peak, and predicts the peak ozone to occur later in the summer than observed following a more typical seasonal cycle. Additionally, at the Northern Europe stations, the measurements indicate that the seasonal ozone maxima occurs in May, whereas the model results lags this seasonal peak with the highest concentrations occurring in June. The modelled summertime ozone bias improves in the Central and Southern Europe stations, with measured and modelled averaged monthly daily maximum ozone concentrations typically within 5 ppb. In Central Europe, the model predicts slightly higher concentrations than observed, particularly in the latter half of the summer. As with the Northern Europe region, the model exhibits a slight shift to the month of peak summer concentrations, with the modelled seasonal cycle lagging the observed cycle by approximately one month. In Southern Europe, the model also exhibits a slight bias to the summertime concentrations of about 5 ppb and the same seasonal shift to the ozone concentrations.

GMDD
5, 149–188, 2012

Interestingly, the modelled seasonal cycle exhibits slight interannual variability compared to the observations. The unusual heat wave event of August 2003 is evident in the observations, particularly at the eight representative sites and the Central Europe and Southern Europe stations. While the model simulates the ozone event of this year fairly well, concentrations in other years are frequently higher than observed, particularly at several of the Central European stations. This lack of strong interannual variability is currently being explored with separate simulations in the European and other regional domains.

5 Conclusions and recommendations

In this paper, we describe a newly developed, online, integrated chemistry-climate model (RegCM-CHEM4) designed to conduct high-resolution, long-term simulations of climate and tropospheric ozone. We provide evidence that the RegCM-CHEM4 can simulate event-driven ozone concentrations in August 2003 as well as a long-term seasonal cycle of ozone. For the August 2003 event analysis, we find that the model is able to reproduce the overall diurnal cycle of ozone and the sharp shifts in concentrations due to meteorological conditions. Analysis of the full six years of simulation indicates that the coupled chemistry-climate model can reproduce the seasonal cycle of ozone, with an overestimation of ozone in the non-event years of 5–15 ppb depending on the geographic region.

In this manuscript, we neglect the feedbacks from the radiative forcing of ozone, essentially decoupling the atmospheric chemistry and dynamics, a feedback that will be discussed in subsequent manuscripts. Future model evaluation tasks will include an assessment of the radiative forcing produced by ozone in these simulations, the impacts of online chemistry on the simulation of atmospheric aerosols in the RegCM-CHEM4 aerosol tracer model, and the effects of using non-climatological chemical boundary conditions for decadal scale simulations. Future model development tasks include the addition of a full thermodynamic aerosol model to replace or use in

GMDD
5, 149–188, 2012

conjunction with the existing RegCM4 aerosol transport scheme (Giorgi et al., 2012), and the development of wet removal by the cumulus precipitation parameterization. Despite these model limitations and the need for additional simulations and evaluation over other regions of the globe, the results presented here show that the model can perform accurate simulations of regional ozone for use in chemistry-climate studies. Future studies will investigate the model over other domains and conditions, with the intent of performing decadal scale simulations of ozone, model intercomparisons with other regional chemistry-climate models, and improving the representation of interannual ozone variability.

Acknowledgement. This work was supported with a grant from the US-Egypt Joint Science and Technology Fund to A. Zakey and A. L. Steiner (NSF AGS-0809255). We thank the International Centre for Theoretical Physics, Trieste, Italy and the Earth System Physics group for providing administrative and computational support for this project. Participation of R. A. Zaveri in this study was partially supported by the US Department of Energy's (DOE) Atmospheric System Research (ASR) program. We also gratefully acknowledge Louisa Emmons at NCAR for providing MOZART chemical boundary conditions for these simulations.

References

Barth, M. C., Sillman, S., Hudman, R., Jacobson, M. Z., Kim, C.-H., Monod, A., and Liang, J.: Summary of the cloud chemistry modelling intercomparisons: photochemical box model simulation, J. Geophys. Res., 108, D7,4214, 2002.

Beekmann, M. and Vautard, R.: A modelling study of photochemical regimes over Europe: robustness and variability, Atmos. Chem. Phys., 10, 10067–10084, doi:10.5194/acp-10-10067-2010, 2010.

Beniston, M. and Diaz, H. F.: The 2003 heat wave as an example of summers in a greenhouse climate? Observations and climate model simulations for Basel, Switzerland, Global Planet. Change, 44, 73–81, 2004.

Black, E., Blackburn, M., Harrison, G., Hoskins, B., and Methven, J.: Factors contributing to the summer 2003 European heat wave, Weather, 59, 217–223, doi:10.1256/wea.74.04, 2004.

GMDD

5, 149–188, 2012

Chang, J., Chang, J. S., Brost, R. A., Isaksen, I. S. A., Madronich, S., Middleton, P., Stockwell, W. R., and Walcek, C. .: A three-dimensional Eulerian and deposition model, Physical concepts and formulation, J. Geophys. Res., 92, 14681–14700, 1987.

Chen, J., Avise, J., Lamb, B., Salathé, E., Mass, C., Guenther, A., Wiedinmyer, C., Lamarque, J.-F., O'Neill, S., McKenzie, D., and Larkin, N.: The effects of global changes upon regional ozone pollution in the United States, Atmos. Chem. Phys., 9, 1125–1141, doi:10.5194/acp-9-1125-2009, 2009.

Dee, D. P., Uppala, S. M., Simmons, A. J., Berrisford, P., Poli, P., Kobayashi, S., Andrae, U., Balmaseda, M. A., Balsamo, G., Bauer, P., Bechtold, P., Beljaars, A. C. M., van de Berg, L., Bidlot, J., Bormann, N., Delsol, C., Dragani, R., Fuentes, M., Geer, A. J., Haimberger, L., Healy, S. B., Hersbach, H., Holm, E. V., Isaksen, L., Kallberg, P., Kohler, M., Matricardi, M., McNally, A. P., Monge-Sanz, B. M., Morcrette, J. J., Park, B. K., Peubey, C., de Rosnay, P., Tavolato, C., Thepaut, J. N., and Vitart, F.: The ERA-Interim reanalysis: configuration and performance of the data assimilation system, Q. J. Roy. Meteorol. Soc., 137, 553–597, 2011.

Emmons, L. K., Walters, S., Hess, P. G., Lamarque, J.-F., Pfister, G. G., Fillmore, D., Granier, C., Guenther, A., Kinnison, D., Laepple, T., Orlando, J., Tie, X., Tyndall, G., Wiedinmyer, C., Baughcum, S. L., and Kloster, S.: Description and evaluation of the Model for Ozone and Related chemical Tracers, version 4 (MOZART-4), Geosci. Model Dev., 3, 43–67, doi:10.5194/gmd-3-43-2010, 2010.

Fast, J. D. and Heilman, W. E.: Simulated sensitivity of seasonal ozone exposure in the Great Lakes region to changes in anthropogenic emissions in the presence of interannual variability, Atmos. Environ., 39, 5291–5306, 2005.

Fast, J. D., Zaveri, R. A., Bian, X., Chapman, E. G., and Easter, R. C.: Effect of regional-scale transport on oxidants in the vicinity of Philadelphia during the 1999 NE-OPS field campaign, J. Geophys. Res., 107(D16), 4330, doi:10.1029/2001JD000980, 2002.

Fast, J. D., Gustafson Jr., W. I., Easter, R. C., Zaveri, R. A., Barnard, J. C., Chapman, E. G., Grell, G. A., and Peckham, S. E.: Evolution of ozone, particulates, and aerosol direct radiative forcing in the vicinity of Houston using a fully coupled meteorology-chemistry-aerosol model, J. Geophys. Res., 111, D21305, doi:10.1029/2005JD006721, 2006.

Fink, A. H., Brücher, T., Krüger, A., Lechebusch, C., Pinto, J. G., and Ulbrich, U.: The 2003 European summer heatwaves and drought-synoptic diagnosis and impacts, Weather, 59, 295–261, doi:10.1256/wea.73.04, 2004.

Forkel, R. and Knoche, R.: Regional climate change and its impact on photooxidant concentra-

GMDD
5, 149–188, 2012

tions in Southern Germany: simulations with a coupled regional climate-chemistry model, J. Geophys. Res., 111, D12302, doi:10.1029/2005JD006748, 2006.
Gery, M. W., Whitten, G. Z., Killus, J. P., and Dodge, M. C.: A photochemical kinetic mechanism for urban and regional scale computer modelling, J. Geophys. Res., 94, 12925–12956, 1989.
Giorgi, F. and Chameides, W. L.: Rainout lifetimes of highly soluble aerosols and gases as inferred from simulations with a general circulation model. J. Geophys. Res., 91, 14367–14376, 1986.
Giorgi, F. and Mearns, L. O.: Introduction to special section: regional climate modeling revisited, J. Geophys. Res., 104, 6335–6352, 1999.
Giorgi, F. and Meleux, F.: Modelling the regional effects of climate change on air quality, C. R. Geoscience, 339, 721–733, 2007.
Giorgi, F. and Shields, C.: Tests of precipitation parameterizations available in the latest version of the NCAR regional climate model (RegCM) over the Continental United States, J. Geophys. Res., 104, 6353–6375, 1999.
Giorgi, F., Pal, J. S., Bi, X., Sloan, L., Elguindi, N., and Solmon, F.: Introduction to the TAC Special Issue: the RegCNET network, Theor. Appl. Climatol., 86, 1–4, 2006.
Giorgi, F., Coppola, E., Solmon, F., Mariotti, L., Sylla, M. B., Elguindi, N., Diro, G. T., Nair, V., Guiliani, S., Cozzini, S., Guettler, I., O'Brien, T. A., Tawfik, A. B., Shalaby, A., Zakey, A. S., Steiner, A. L., Stordal, F., Sloan, L. C., and Brankovic, C.: RegCM4: Model description and preliminary tests over multiple CORDEX domains, in press, doi:10.3354/cr01018, 2012.
Grell, G. A.: Prognostic evaluation of assumptions used by cumulus parameterizations, Mon. Weather Rev., 121, 764–787, 1993.
Grell, G. A., Peckham, S. E., Schmitz, R., McKeen, S. A., Frost, G., Skamarock, W. C., and Eder, B.: Fully coupled online chemistry within the WRF model, Atmos. Environ., 39, 6957–6975, 2005.
Guenther, A., Karl, T., Harley, P., Wiedinmyer, C., Palmer, P. I., and Geron, C.: Estimates of global terrestrial isoprene emissions using MEGAN (Model of Emissions of Gases and Aerosols from Nature), Atmos. Chem. Phys., 6, 3181–3210, doi:10.5194/acp-6-3181-2006, 2006.
Hedegaard, G. B., Brandt, J., Christensen, J. H., Frohn, L. M., Geels, C., Hansen, K. M., and Stendel, M.: Impacts of climate change on air pollution levels in the Northern Hemisphere with special focus on Europe and the Arctic, Atmos. Chem. Phys., 8, 3337–3367, doi:10.5194/acp-8-3337-2008, 2008.

GMDD
5, 149–188, 2012

Hodzic, A., Vautard, R., Chepfer, H., Goloub, P., Menut, L., Chazette, P., Deuzé, J. L., Apituley, A., and Couvert, P.: Evolution of aerosol optical thickness over Europe during the August 2003 heat wave as seen from CHIMERE model simulations and POLDER data, Atmos. Chem. Phys., 6, 1853–1864, doi:10.5194/acp-6-1853-2006, 2006.

Holtslag, A. A. M. and Boville, B. A.: Local versus nonlocal boundary-layer diffusion in a global climate model, J. Climate, 6, 1825-1842, 1993.

Horowitz, L. W., Walters, S., Mauzerall, D. L., Emmons, L. K., Rasch, P. J., Granier, C., Tie, X., Lamarque, J., Schultz, M. G., Tyndall, G. S., Orlando, J. J., and Brasseur, G. P.: A global simulation of tropospheric ozone and related tracers: description and evaluation of MOZART, version 2, J. Geophys. Res., 108, D24, doi:10.1029/2002JD002853, 2003.

IPCC: Intergovernmental Panel On Climate Change, Climate Change 2007: The Physical Science Basis. Contribution of Working Group I to the Fourth Assessment Report of the IPCC, Cambridge University Press, Cambridge, UK, and New York, USA, 2007.

Jacob, D. J. and Winner, D. A.: Effect of climate change on air quality, Atmos. Environ., 43(1), 51–63, doi:10.1016/j.atmosenv.2008.09.051, 2009.

Jacobson, M. Z.: Development and application of a new air pollution modeling system – Part II: aerosol module structure and design, Atmos. Environ., 31, 131–144, 1997a.

Jacobson, M. Z.: Development and application of a new air pollution modeling system – Part III: aerosol-phase simulation, Atmos. Environ., 31, 587–608, 1997b.

Jacobson, M. Z., Lu, R., Turco, R. P., and Toon, O. B.: Development and application of a new air pollution modeling system – Part I: gas-phase simulation, Atmos. Environ., 30, 1939–1963, 1996.

Jiang, G. and Fast, J. D.: Modeling the effects of VOC and NO_x emission sources on ozone formation in Houston during the TexAQS 2000 field campaign, Atmos. Environ., 38, 5071–5085, 2004.

Kiehl, J. T., Hack, J. J., Bonan, G. B., Boville, B. A., Breigleb, B. P., Williamson, D., and Rasch, P.: Description of the NCAR community climate model (CCM3), Tech. Rep. NCAR/TN-420+STR, National Center for Atmospheric Research, , 1996.

Krüger, B. C., Katragkou, E., Tegoulias, I., Zanis, P., Melas, D., Coppola, E., Rauscher, S., Huszar, P., and Halenka, T.: Regional photochemical model calculations for Europe concerning ozone levels in a changing climate, Q. J. Hung. Met. Serv., 112, 285–300, 2008.

Lamarque, J.-F., Bond, T. C., Eyring, V., Granier, C., Heil, A., Klimont, Z., Lee, D., Liousse, C., Mieville, A., Owen, B., Schultz, M. G., Shindell, D., Smith, S. J., Stehfest, E., Van Aar-

GMDD
5, 149–188, 2012

denne, J., Cooper, O. R., Kainuma, M., Mahowald, N., McConnell, J. R., Naik, V., Riahi, K., and van Vuuren, D. P.: Historical (1850–2000) gridded anthropogenic and biomass burning emissions of reactive gases and aerosols: methodology and application, Atmos. Chem. Phys., 10, 7017–7039, doi:10.5194/acp-10-7017-2010, 2010.

Langner, J., Bergström, R., and Foltescu, V.: Impact of climate change on surface ozone and deposition of sulphur and nitrogen in Europe, Atmos. Environ., 39, 1129–1141, 2005

Leibensperger, E. M., Mickley, L. J., and Jacob, D. J.: Sensitivity of US air quality to mid-latitude cyclone frequency and implications of 1980–2006 climate change, Atmos. Chem. Phys., 8, 7075–7086, doi:10.5194/acp-8-7075-2008, 2008.

Madronich, S. and Flocke, S.: The role of solar radiation in atmospheric chemistry, in: Handbook of Environmental Chemistry, edited by: Boule, P., Springer-Verlag, New York, 1–26, 1999.

Meehl, G. A. and Tebaldi, C.: More intense, more frequent and longer lasting heat waves in the 21st century, Science, 305, 994–997, 2004.

Meleux, F., Solmon, F., and Giorgi, F.: Increase in summer European ozone amounts due to climate change, Atmos. Environ., 41, 7577–7587, 2007.

Milford, J., Gao, D., Sillman, S., Blossey, P., and Russell, A. G.: Total reactive nitrogen (NO_y) as an indicator for the sensitivity of ozone to NO_x and hydrocarbons, J. Geophys. Res., 99, 3533–3542, 1994.

Mitchell, T. D. and Jones, P. D.: An improved method of constructing a database of monthly climate observations and associated high-resolution grids, Int. J. Climatol., 25, 693–712, doi:10.1002/joc.1181, 2005.

Neuman, J. A., Parrish, D. D., Trainer, M., Ryerson, T. B., Holloway, J. S., Nowak, J. B., Swanson, A., Flocke, F., Roberts, J. M., Brown, S. S., Stark, H., Sommariva, R., Stohl, A., Peltier, R., Weber, R., Wollny, A. G., Sueper, D. T., Hubler, G., and Fehsenfeld, F. C.: Reactive nitrogen transport and photochemistry in urban plumes over the North Atlantic Ocean, J. Geophys. Res., 111, D23S54, doi:10.1029/2005JD007010, 2006.

Ordóñez, C., Mathis, H., Furger, M., Henne, S., Hüglin, C., Staehelin, J., and Prévôt, A. S. H.: Changes of daily surface ozone maxima in Switzerland in all seasons from 1992 to 2002 and discussion of summer 2003, Atmos. Chem. Phys., 5, 1187–1203, doi:10.5194/acp-5-1187-2005, 2005.

Oleson, K. W., Niu, G.-Y., Yang, Z.-L., Lawrence, D. M., Thornton, P. E., Lawrence, P. J., Stockli, R., Dickinson, R. E., Bonan, G. B., Levis, S., Dai, A., and Qian, T.: Improvements

GMDD
5, 149–188, 2012

to the Community Land Model and their impact on the hydrological cycle, J. Geophys. Res., 113, G01021, doi:10.1029/2007JG000563, 2008.
Pal, J. S., Small, E. E., and Eltahir, E. A. B.: Simulation of regional-scale water and energy budgets: representation of subgrid cloud and precipitation processes within RegCM, J. Geophys. Res.-Atmos. 105(D24), 29579–29594, 2000.
Pal, J. S., Giorgi, F., Bi, X., Elguindi, N., Solmon, F., Gao, X. J., Francisco, R., Zakey, A., Winter, J., Ashfaq, M., Syed, F., Bell, J., Diffenbaugh, N., Karmacharya, J., Konare, A., Martinez-Castro, D., Porfirio da Rocha, R., Sloan, L., and Steiner, A.: Regional climate modeling for the developing world: The ICTP RegCM3 and RegCNET, B. Am. Meteorol. Soc., 88, 1395–1409, 2007.
Qian, Y. and Giorgi, F.: Interactive coupling of regional climate and sulfate aerosol models over Eastern Asia, J. Geophys. Res., 104, 6477–6499, 1999.
Schär, C., Vidale, P. L., Lüthi, D., Frei, C., Häberli, C., Liniger, M. A., and Appenzeller, C.: The role of increasing temperature variability in European summer heatwaves, Nature, 427, 332–336, 2004.
Sillman, S.: A numerical solution for equations of tropospheric chemistry based on an analysis of sources and sinks of odd hydrogen, J. Geophys. Res., 96, 20735–20744, 1991.
Sillman, S. and He, D.: Some theoretical results concerning O_3-NO_x-VOC chemistry and NO_x-VOC indicators, J. Geophys. Res., 107, D22, 4659, doi:10.1029/2001JD001123, 2002.
Sillman, S., Samson, P. J., and Masters, J. M.: Ozone formation in urban plumes transported over water: photochemical model and case studies in the Northeastern and Midwestern US, J. Geophys. Res., 98, 12687–12699, 1993.
Solberg, S., Hov, Ø., Søvde, A., Isaksen, I. S. A., Coddeville, P., De Backer, H., Forster, C., Orsolini, Y., and Uhse, K.: European surface ozone in the extreme summer 2003, J. Geophys. Res., 113, D7, doi:10.1029/2007JD009098, 2008.
Solmon, F., Giorgi, F., and Liousse, C.: Aerosol modelling for regional climate studies: application to anthropogenic particles and evaluation over a European/African domain, Tellus B, 58, 51–72, 2006.
Stamnes, K., Henriksen, K., and Østensen, P.: Simultaneous measurement of UV radiation received by the biosphere and total ozone amount, Geophys. Res. Lett., 15(8), 784–787, 1988.
Steiner, A. L., Tonse, S., Cohen, R. C., Goldstein, A. H., and Harley, R. A.: The influence of future climate and emissions on regional air quality in California, J. Geophys. Res., 111,

GMDD
5, 149–188, 2012

D18303, doi:10.1029/2005JD006935, 2006.
Stevenson, D. S., Doherty, R. M., Sanderson, M. G., Johnson, C. E., Collins, W. J., and Derwent, R. G.: Impacts of climate change and variability on tropospheric ozone and its precursors, Faraday Discuss., 130, 41–57, 2005.
Struzewska, J. and Kaminski, J. W.: Formation and transport of photooxidants over Europe during the July 2006 heat wave – observations and GEM-AQ model simulations, Atmos. Chem. Phys., 8, 721–736, doi:10.5194/acp-8-721-2008, 2008.
Szopa, S., Hauglustaine, D., Vautard, R., and Menut, L.: Evaluation of the tropospheric composition in 2030: impact on European air quality, Geophys. Res. Lett., 33, L14805, 2006.
Tawfik, A. B. and Steiner, A. L.: The role of soil ice in land-atmosphere coupling over the United States: a soil moisture-precipitation winter feedback mechanism, JGR Atmos., 116, D02113, doi:10.1029/2010JD014333, 2011.
Tawfik, A. B., Stöckli, R., Goldstein, A. H., Pressley, S. L., and Steiner, A. L.: Quantifying the contribution of environmental factors to isoprene flux interannual variability, Atmos. Environ., in review, 2012.
Vautard, R., Honoré, C., Beekmann, M., and Rouil, L.: Simulation of ozone during the August 2003 heat wave and emission control scenarios, Atmos. Environ., 39, 2957–2967, 2005.
Vogel, B., Riemer, N., Vogel H., Fiedler, F.: Findings on NO_y as an indicator for ozone sensitivity based on different numerical simulations, J. Geophys. Res., 104, D3, 3605–3620, doi:10.1029/1998JD100075, 1999.
Weaver, C. P., Cooter, E., Gilliam, R., Gilliland, A., Grambsch, A., Grano, D., Hemming, B., Hunt, S. W., Nolte, C., Winner, D. A., Liang, X-Z., Zhu, J., Caughey, M., Kunkel, K., Lin, J.-T., Tao, Z., Williams, A., Wuebbles, D.J., Adams, P. J., Dawson, J. P., Amar, P. He, S., Avise, J., Chen, J., Cohen, R.C., Goldstein, A.H., Harley, R. A., Steiner, A. L., Tonse, S., Guenther, A., Lamarque, J.-F., Wiedinmyer, C., Gustafson, W. I., Leung, L. R., Hogrefe, C., Huang, H.-C., Jacob, D. J., Mickley, L. J., Wu, S., Kinney, P. L., Lamb, B., Larkin, N. K., McKenzie, D., Liao, K-J., Manomaiphiboon, K., Russel, A. G., Tagaris, E., Lynn, B. H., Mass, C., Salathe, E., O'Neill, S. M., Pandis, S. N., Racherla, P. N. Rosenzweig, C., and Woo, J-H.: A preliminary synthesis of modelled climate change impacts on US regional ozone concentrations, B. Am. Meteorol. Soc., 90, 12, 1843–1863, 2009.
Wesely, M. L.: Parameterization of surface resistance to gaseous dry deposition in regional-scale numerical models, Atmos. Environ., 23, 1293–1304, 1989.
WHO: The health impacts of 2003 summer heat-waves. Briefing note for the Delegations of the

GMDD
5, 149–188, 2012

fifty-third session of the WHO (World Health Organization) Regional Committee for Europe, 12 pp., 2003.

Zaveri, R. and Peters, L. K.: A new lumped structure photochemical mechanism for large-scale applications, J. Geophys. Res., 104, 30387–30415, 1999.

Zaveri, R. A., Berkowitz, C. M., Kleinman, L. I., Springston, S. R., Doskey, P. V., Lonneman, W. A., and Spicer, C. W.: Ozone production efficiency and NO_x depletion in an urban plume: interpretation of field observations and implications for evaluating O_3-NO_x-VOC sensitivity, J. Geophys. Res., 108(D14), 4436, doi:10.1029/2002JD003144, 2003.

Zaveri, R. A., Berkowitz, C. M., Brechtel, F. J., Gilles, M. K., Hubbe, J. M., Jayne, J. T., Kleinman, L. I., Laskin, A., Madronich, S., Onasch, T. B., Pekour, M. S., Springston, S. R., Thornton, J. A., Tivanski, A. V., and Worsnop, D. R: Nighttime chemical evolution of aerosol and trace gases in a power plant plume: implications for secondary organic nitrate and organosulfate aerosol formation, NO_3 radical chemistry, and N_2O_5 heterogeneous hydrolysis, J. Geophys. Res., 115, D12304, doi:10.1029/2009JD013250, 2010a.

Zaveri, R. A., Voss, P. B., Berkowitz, C. M., Fortner, E., Zheng, J., Zhang, R., Valente, R. J., Tanner, R. L., Holcomb, D., Hartley, T. P., and Baran, L: Overnight atmospheric transport and chemical processing of photochemically aged Houston urban and petrochemical industrial plume, J. Geophys. Res., 115, D23303, doi:10.1029/2009JD013495, 2010b.

Zhang, Y.: Online-coupled meteorology and chemistry models: history, current status, and outlook, Atmos. Chem. Phys., 8, 2895–2932, doi:10.5194/acp-8-2895-2008, 2008.

Zhang, Y., Hu, X.-M., Leung, L. R., and Gustafson Jr., W. I.: Impact of regional climate changes on biogenic emissions and air quality, J. Geophys. Res., 113, D18310, doi:10.1029/2008JD009965, 2008.

Zhang, Y., Wen, X.-Y., and Jang, C. J.: Simulating climate-chemistry-aerosol-cloud-radiation feedbacks in Continental US using online-coupled WRF/Chem, Atmos. Environ., 44(29), 3568–3582, 2010.

GMDD

5, 149–188, 2012

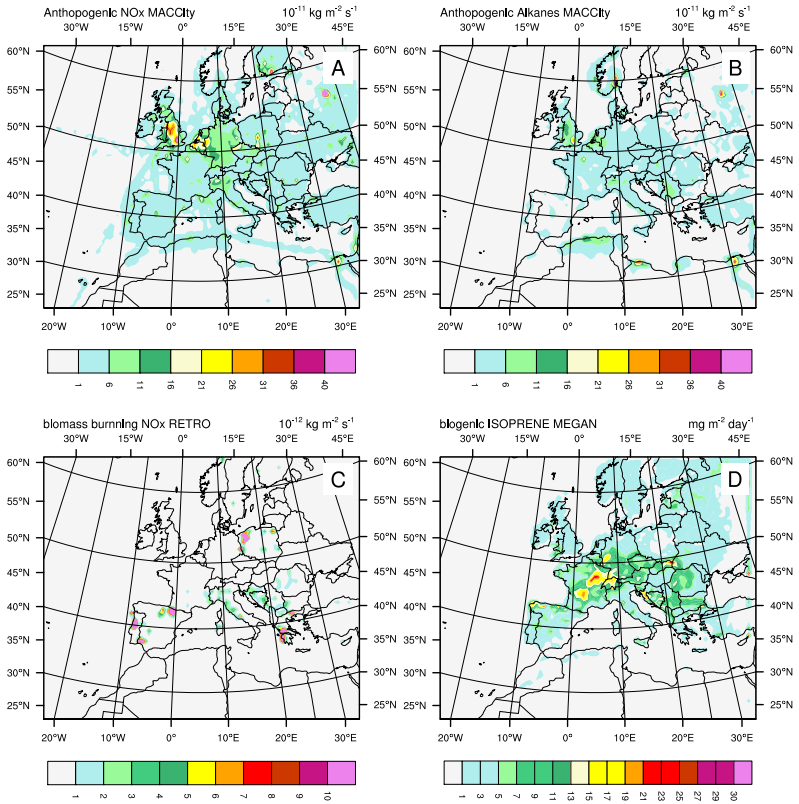

Fig. 1. Model domain and selected emissions used in RegCM-CHEM4, **(a)** NO_x MACCity anthropogenic emissions (10^{-11} kg m^{-2} s^{-1}), **(b)** anthropogenic MACCity alkane emissions (10^{-11} kg m^{-2} s^{-1}), **(c)** NO_x biomass burning emissions from the RETRO inventory (10^{-11} kg m^{-2} s^{-1}), and **(d)** biogenic isoprene emissions calculated online with the MEGAN model (mg m^{-2} d^{-1}).

GMDD
5, 149–188, 2012

Implementation and evaluation of online gas-phase chemistry

A. K. Shalaby et al.

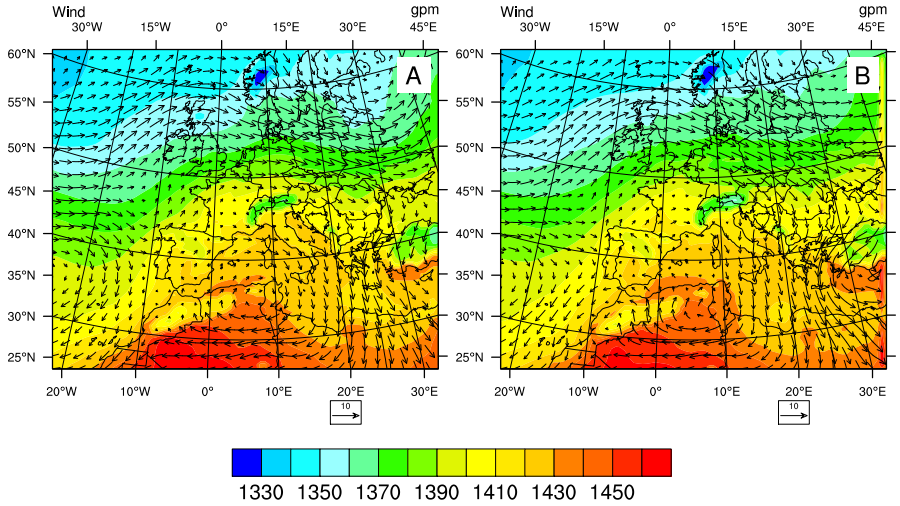

Fig. 2. **(a)** ERA-Interim Reanalysis of 850 mb geopotential surface and wind field averaged over August 2003. **(b)** RegCM-CHEM4 850 mb geopotential surface and wind field averaged over August 2003.

GMDD
5, 149–188, 2012

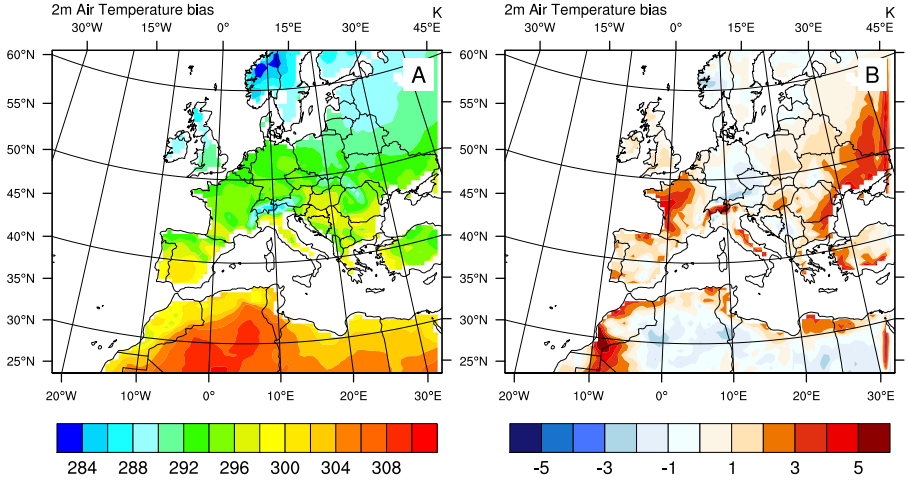

Fig. 3. **(a)** RegCM-CHEM4 average surface air temperature (K) and **(b)** August 2003 model surface air temperature bias, based on CRU data (Mitchell and Jones, 2005).

GMDD
5, 149–188, 2012

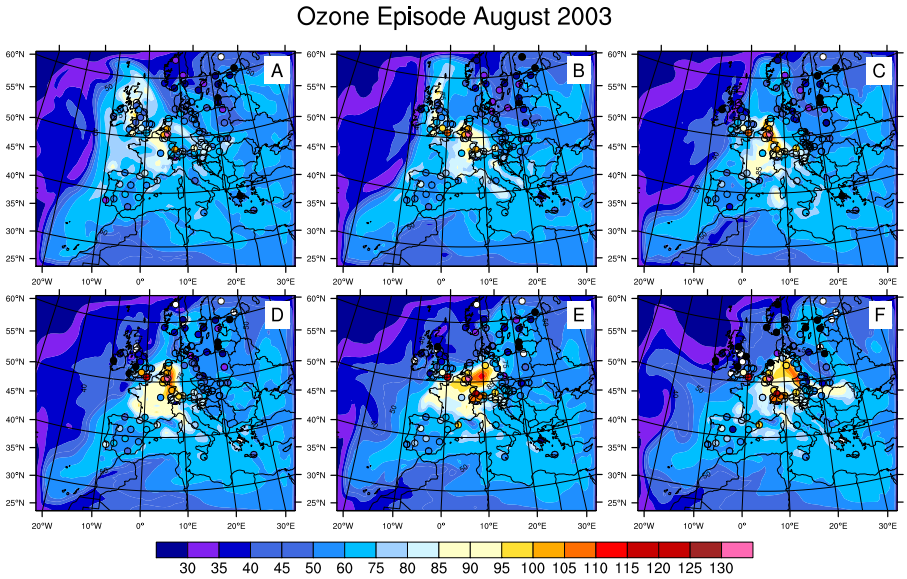

Fig. 4. Evolution of the ozone concentration field through the first two weeks of August 2003 corresponding to the core of the August 2003 heat wave. Each panel displays a concentration field in ppb at 14 h UT. **(a)** 1 August, **(b)** 4 August, **(c)** 8 August, **(d)** 10 August, **(e)** 12 August, **(f)** 16 August. EMEP station locations are shown in circles with observed ozone concentrations (color of circle following contour legend).

GMDD
5, 149–188, 2012

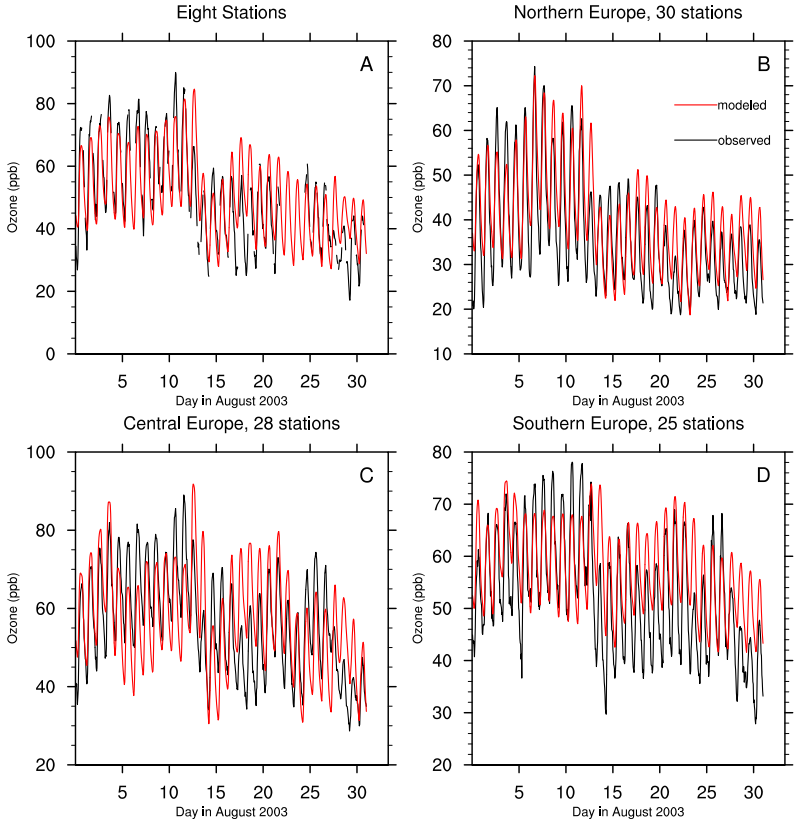

Fig. 5. Measured (black) and modelled (red) surface ozone concentrations (ppb) for **(a)** eight representative EMEP stations (see text for locations), **(b)** 30 EMEP stations in Northern Europe (latitudes greater than 50° N), **(c)** 28 EMEP stations in Central Europe (latitudes 47–50° N), and **(d)** 25 stations in Southern Europe (latitudes less than 47° N).

GMDD
5, 149–188, 2012

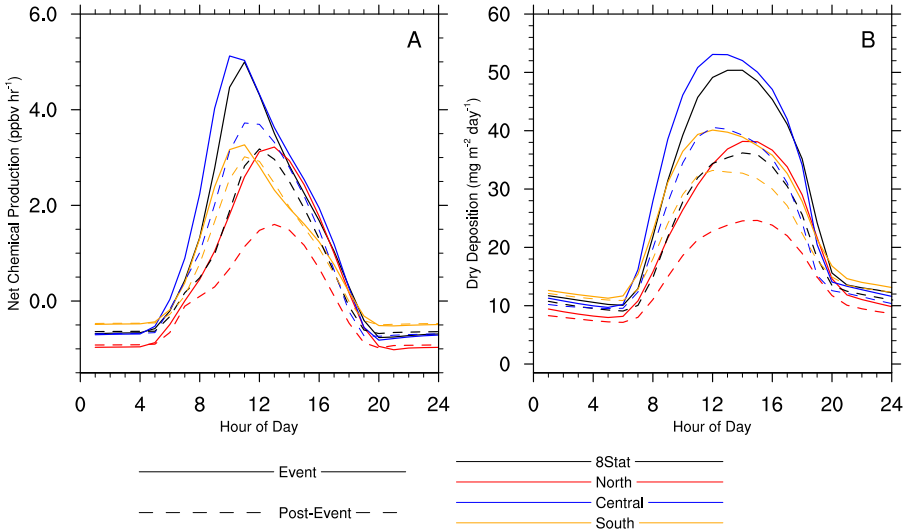

Fig. 6. (a) Average diurnal cycle of modeled rates of net chemical production (ozone production – ozone loss; ppb h^{-1}) for the four regions of analysis (as in Fig. 5, Sect. 3.3) for the ozone event (1–14 August 2003; solid lines) and after the ozone event (16–31 August 2003; dashed lines). **(b)** As for **(a)**, but for dry deposition rates (mg m^{-2} day^{-1}). Wet deposition rates were zero over this month.

GMDD
5, 149–188, 2012

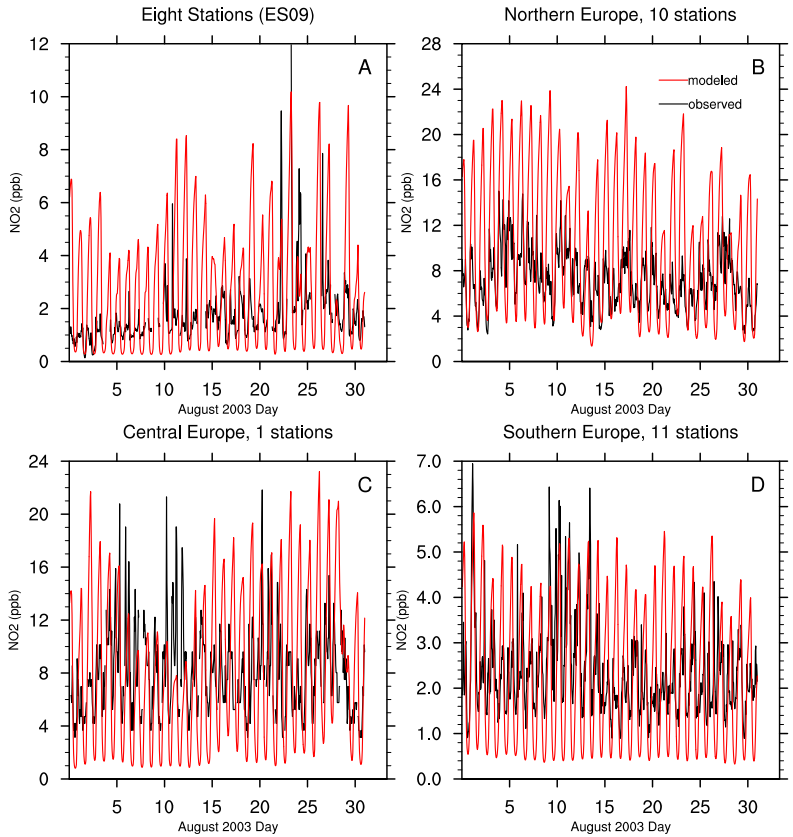

Fig. 7. Measured (black) and modelled (red) surface NO_2 concentrations (ppb) for **(a)** one of the eight representative EMEP stations (ES09), **(b)** 10 EMEP stations in Northern Europe (latitudes greater than 50° N), **(c)** 1 EMEP station in Central Europe (latitudes 47–50° N), and **(d)** 11 stations in Southern Europe (latitudes less than 47° N).

GMDD
5, 149–188, 2012

Implementation and evaluation of online gas-phase chemistry

A. K. Shalaby et al.

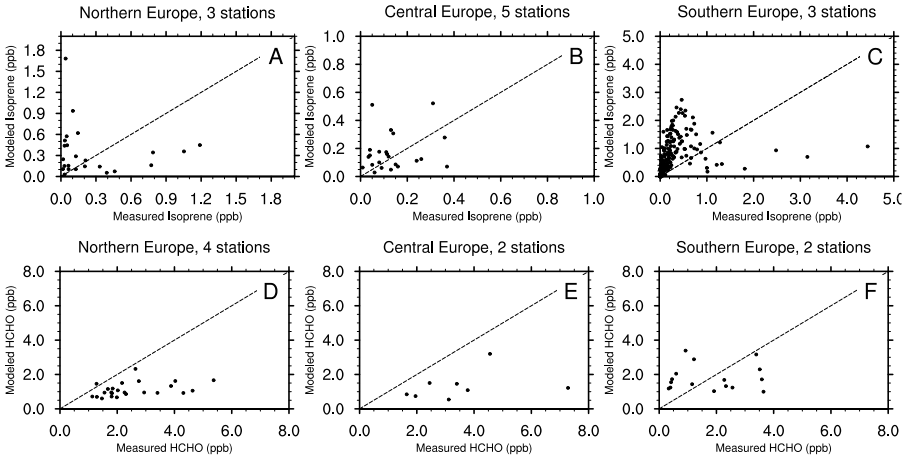

Fig. 8. Scatter plots of measured versus modelled isoprene (ppb) for **(a)** 3 stations in Northern Europe, **(b)** 5 stations in Central Europe and **(c)** 3 stations in Southern Europe, and measured versus modelled formaldehyde (ppb) for **(d)** 4 stations in Northern Europe, **(e)** 2 stations in Central Europe, and **(f)** 2 stations in Southern Europe.

GMDD
5, 149–188, 2012

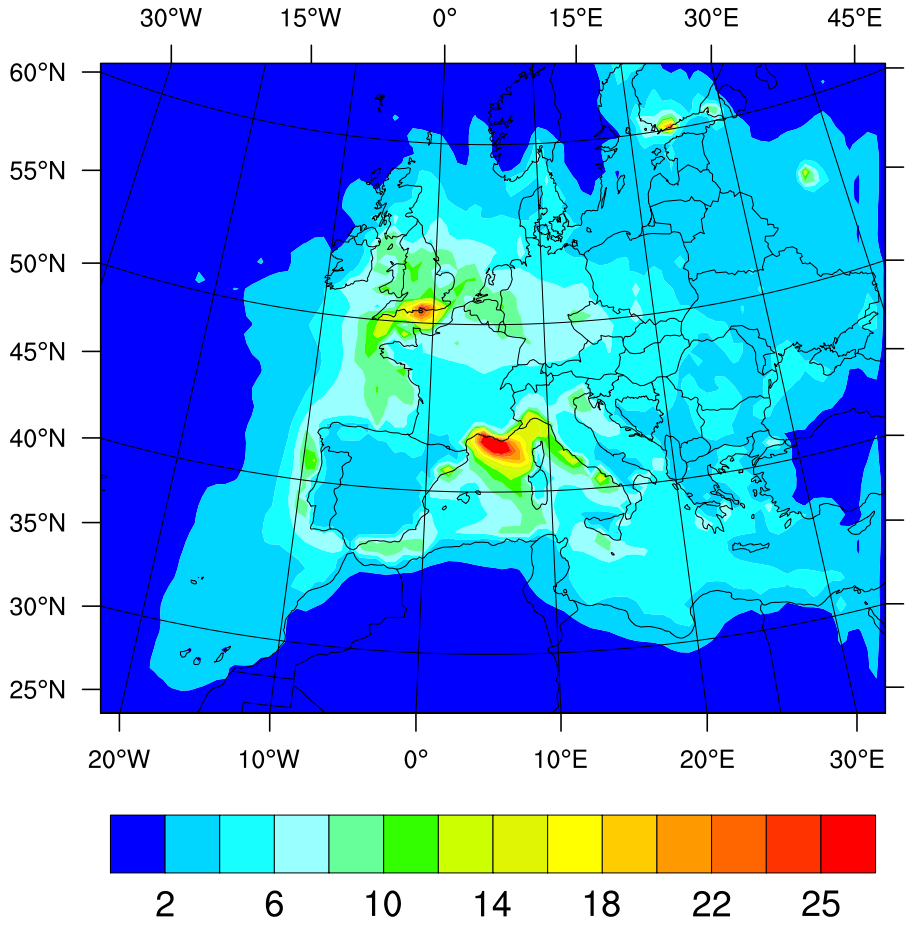

Fig. 9. Average August 14:00 (UT) 2003 concentration of NO_y (ppb).

GMDD
5, 149–188, 2012

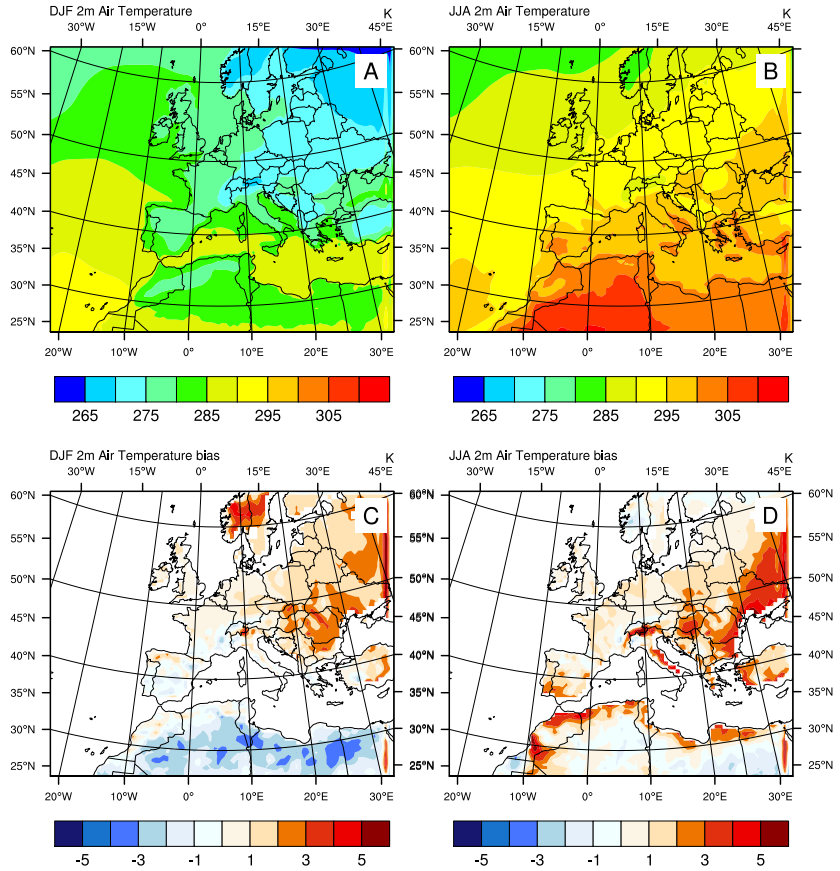

Fig. 10. **(a)** RegCM-CHEM4 modelled climatological average surface air temperature (K) for DJF (2000–2005) **(b)** JJA (2000–2005). Model temperature bias for **(c)** DJF and **(d)** JJA based on CRU data (Mitchell and Jones, 2005).

GMDD
5, 149–188, 2012

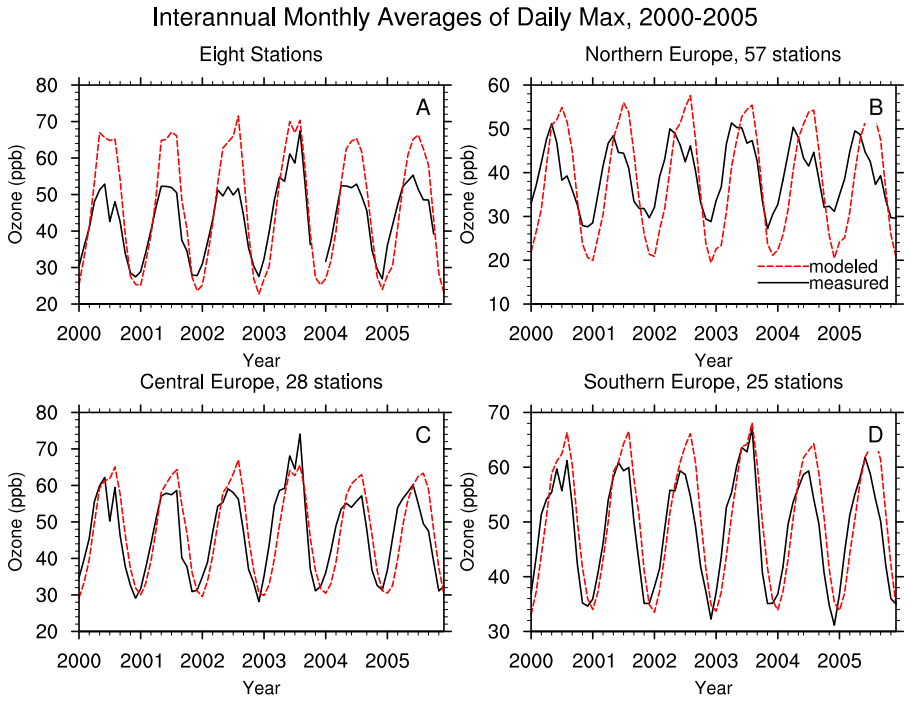

Fig. 11. Monthly average of daily maximum surface ozone concentrations (ppb) as measured (black) and modelled (red) for **(a)** eight representative EMEP stations (see text for locations), **(b)** 57 EMEP stations in Northern Europe, **(c)** 28 EMEP stations in Central Europe and **(d)** 25 stations in Southern Europe.

GMDD
5, 149–188, 2012